# Free energy surface reconstruction from umbrella samples using Gaussian process regression II: Multiple collective variables

Thomas Stecher,*,† Noam Bernstein,‡ and Gábor Csányi*,†

*Department of Engineering, University of Cambridge, Trumpington Street, Cambridge, CB2 1PZ, UK, and Naval Research Laboratory, Center for Computational Materials Science, Washington, DC 20375, United States of America*

E-mail: thomas.stecher@tum.de; gc121@cam.ac.uk

**Abstract**

We demonstrate how a prior assumption of smoothness can be used to enhance the reconstruction of free energy profiles from multiple umbrella sampling simulations using the Bayesian Gaussian process regression approach. The method we derive allows the concurrent use of histograms and free energy gradients and can easily be extended to include further data. In Part I we review the necessary theory and test the method for one collective variable. We demonstrate improved performance with respect to the weighted histogram analysis method and obtain meaningful error bars without any significant additional computation. In Part II we consider the case of multiple collective variables and compare to a reconstruction using least squares fitting of radial basis functions. We find substantial improvements in the regimes of spatially sparse

†To whom correspondence should be addressed

†Department of Engineering, University of Cambridge, Trumpington Street, Cambridge, CB2 1PZ, UK

‡Naval Research Laboratory, Center for Computational Materials Science, Washington, DC 20375, United States of America

data or short sampling trajectories. A software implementation is made available on www.libatoms.org.

# 1 Introduction

In Part I we described a Bayesian method for the reconstruction of free energy profiles from umbrella sampling simulations, based on Gaussian process regression (GPR),[1] in which one makes explicit the *a priori* assumption of smoothness of the underlying function, and takes account of the sampling noise in a consistent fashion. In Part I we tested the method in a system with one collective variable. Here we investigate its performance when using derivative information in the case of two and four collective variables.

Working with more than one collective coordinate significantly adds to the challenge of free energy reconstruction. The most obvious additional problem, which gets exponentially more difficult as the number of dimensions increases, is exploration, i.e. the problem of ensuring that the entire region of interest is sufficiently sampled. Some approaches, such as metadynamics[2] and the adaptive biasing force method,[3,4] combine exploration and reconstruction by gradually building up an approximate bias potential that is designed to converge to the negative of the potential of mean force and thus counteract the natural occupancy bias of the Boltzmann distribution towards low free energy regions. Another approach is to separate exploration from reconstruction, as in the single-sweep method.[5] In this approach, temperature-accelerated molecular dynamics (TAMD)[6] – an extension of adiabatic free energy dynamics (AFED)[7,8] – is used in a first step to identify a number of points in the "important regions of the free energy landscape".[5] At these points free energy gradients are calculated using independent standard umbrella sampling simulations and then, finally, the free energy surface is reconstructed from these gradients by a least squares fitting procedure using radial basis functions (LSRBF). Recently, Tuckerman and co-workers[9] proposed what amounts to a synthesis of metadynamics and the single-sweep method, combining dynamics

at higher temperature in the (adiabatically decoupled) collective variables with an on-the-fly construction of a bias potential to steer the system away from regions in collective-variable space already visited. The free energy is again reconstructed from measurements of its gradients in umbrella simulations and least squares fitting.

In the present work, we do not tackle what might seem the more open ended and thus harder first task of exploration; rather, we seek to set up a framework for performing the second task of free energy reconstruction as efficiently as possible. Our main interest in more than one dimension is therefore to see how the GPR(d) formulation compares with the least squares RBF reconstructions that have been used to date. The latter approach is known to have problems with large condition numbers in cases where the data density is high.[5,10] The linear system to be solved in Gaussian process regression, on the other hand, can be expected to be well conditioned because of the addition of the noise covariance matrix to the linear system. Because the simulations needed for exploration and collection of free energy gradients are so computationally expensive, the *post hoc* reconstruction of the free energy surface is a negligible part of the overall computational cost for both the LSRBF reconstruction as well as for the GPR(d) we propose.

# 2 Function reconstruction using gradients in several dimensions

When reconstructing the free energy surface using a least squares fit, the free energy as a function of a $D$-dimensional collective coordinate $f(\mathbf{x}^*)$ is written as a linear combination of basis functions centred on the data points,

$$f(\mathbf{x}^*) = \sum_{i=1}^{n} a_i k(\mathbf{x}^*, \mathbf{x}_i'), \tag{1}$$

where $n$ is the number of data points, $\mathbf{x}'_i$ are the set of collective coordinates of the data, $k(\mathbf{x}^*, \mathbf{x}'_i)$ are basis functions centred on $\mathbf{x}'_i$, and $a_i$ are their coefficients. The particular collective variables used in Sec. 3 are dihedral angles, which are periodic, so in order to construct suitable basis functions we use the periodic generalisation of the squared exponential (SE) kernel† from Part I, given by[11]

$$k(x_1, x_2) = \sigma_f^2 \exp\left(-\frac{2\left|\sin\left(\frac{\mathbf{x}_1-\mathbf{x}_2}{2}\right)\right|^2}{l^2}\right), \tag{2}$$

where the sine function applied to a vector is to be interpreted element-wise. In LSRBF, the coefficients, $a_i$, are then obtained by minimising the following error function, given by the sum of the squared deviations of the reconstructed gradients from the observed gradients,

$$E(\mathbf{a}) = \sum_{i=1}^{n} \left| \sum_{j=1}^{n} a_j \boldsymbol{\nabla}_{\mathbf{x}'_i} k(\mathbf{x}'_i, \mathbf{x}'_j) - \mathbf{y}'_i \right|^2, \tag{3}$$

where $\mathbf{y}'_i$ are the observed (noisy) free energy gradients. Like all least squares problems, this minimisation can be reduced to a linear algebraic system with the following solution:[5]

$$\mathbf{a} = (\boldsymbol{\nabla}\mathbf{k}^T \boldsymbol{\nabla}\mathbf{k})^{-1} \boldsymbol{\nabla}\mathbf{k}^T \mathbf{y}', \tag{4}$$

where $\mathbf{y}'$ is a vector obtained by concatenating all the measured gradients (such that $y'_{iD+\alpha}$ is the $\alpha^{\text{th}}$ element of $\mathbf{y}'_i$, where $D$ is the number of dimensions) and $\boldsymbol{\nabla}\mathbf{k}$ is a $nD \times n$ matrix containing the gradients of all basis functions at all centres such that $(\boldsymbol{\nabla}\mathbf{k})_{iD+\alpha,j}$ is the $\alpha^{\text{th}}$ element of $\boldsymbol{\nabla}_{\mathbf{x}'_i} k(\mathbf{x}'_i, \mathbf{x}'_j)$. Maragliano and Vanden-Eijnden further suggest optimising the length scale (hyper-) parameter, $l$, by minimising the residual $E(\mathbf{a})$.[5] We show below that this can lead to inferior results compared to setting a length-scale informed by our *a priori* knowledge about the system.

†We use the designation "SE" for the kernel instead of the more common name "Gaussian" in order to distinguish it from the multivariate Gaussian probability distribution that underlies Gaussian process regression. The GPR formalism can be used with any positive definite kernel, of which the Gaussian or SE kernel is just one possibility.

The GPR(d) solution also uses an ansatz similar to (1), but differs from the above in the following important respects: the nature and number of the basis functions, and the way the coefficients are calculated. The first point was briefly addressed for the 1D case in Part I: the basis functions used in the GPR(d) reconstruction are not the original SE kernels, $k(\mathbf{x}^*, \mathbf{x}'_i)$, with peaks at their centres, $x^* = x'_i$, but rather their gradients,

$$k_{f,f'_\alpha}(\mathbf{x}^*, \mathbf{x}'_i) = \frac{\partial}{\partial x'_{i,\alpha}} k(\mathbf{x}^*, \mathbf{x}'_i), \tag{5}$$

which evaluate to zero at the centres and instead have a strong linear component there. (The index $\alpha$ indicates the direction of differentiation). The interpretation of these basis functions is the *a priori* correlation between the measured gradient values and the unknown function values. These basis functions should be better suited to fitting the derivative information, which does not inform us about the absolute function value but only about its slope. The second point, the larger number of basis functions, is unique to the higher-dimensional case: there will be one kernel function in the expansion for every component of the gradient data, rather than just one for each data point. The GPR(d) expansion in terms of kernel functions is thus

$$\bar{f}(\mathbf{x}^*) = \sum_{i=1}^{n} \sum_{\alpha=1}^{D} b_{i,\alpha} k_{f,f'_\alpha}(\mathbf{x}^*, \mathbf{x}'_i). \tag{6}$$

The coefficients $b_{i,\alpha}$ are obtained by the standard GPR expression (cf. Part I)

$$\mathbf{b} = (K_{f',f'} + \Sigma_{y'})^{-1} \mathbf{y}', \tag{7}$$

where $\mathbf{y}'$ is a vector consisting of all the measured gradients (as in Eq. (4), $y'_{iD+\alpha}$ is the $\alpha^{\text{th}}$ element of $\mathbf{y}'_i$), $\Sigma_{y'}$ is a diagonal matrix containing the noise variances associated with the observations $\mathbf{y}'$ and $\mathbf{b}$ is a vector of the coefficients $b_{i,\alpha}$. $K_{f',f'}$ is an $nD \times nD$ matrix

containing the prior covariances between all the partial derivatives, its elements given by

$$[K_{f,f'}]_{iD+\alpha,jD+\beta} = \frac{\partial^2}{\partial x'_{i,\alpha} \partial x'_{j,\beta}} k(\mathbf{x}'_i, \mathbf{x}'_j). \tag{8}$$

The greater flexibility of the Gaussian process afforded by the increased number of basis functions leads to greater variational freedom, but the regularisation due to the Bayesian prior mitigates the risk of overfitting. While the coefficients in the LSRBF approach are calculated to achieve the best possible fit of the data and therefore risk overfitting, GPR(d) takes account both of the noise associated with the input data through $\Sigma_{y'}$ and of the expected similarity of different data points through $K_{f',f'}$. A comparison of Eqs. (4) and (7) shows that both approaches have a computational complexity that scales similarly with the number of data points, requiring the construction of a matrix involving gradients of the kernel, and the inversion of the matrix or the solution of a corresponding linear system.

# 3 Methods

## 3.1 Test system

We compare the two reconstruction methods above in both two and four collective variables. For the former we used the same CHARMM22[12]-model of the alanine dipeptide (N-acetyl-alanine-N'-methylamide; Ace-Ala-Nme) as in Part I (gas phase, NVT ensemble at 300 K controlled by a Langevin thermostat[13] with a damping parameter of 100 fs, time-step of 0.5 fs). The two backbone dihedral angles, $\Phi$ (C-N-$C_\alpha$-C) and $\Psi$ (N-$C_\alpha$-C-N), were used as the collective variables. For the four-dimensional calculations we used the same parameters, but replaced the dipeptide with the CHARMM22-model of the alanine tripeptide (blocked dialanine, Ace-Ala-Ala-Nme) and used its four backbone dihedral angles as collective variables. Once again, we used the LAMMPS[14] package together with the PLUMED[15] library to carry out the calculations.

For our tests on the alanine dipeptide we collected data on an evenly spaced grid of $48 \times 48$ centres with an umbrella strength of $\kappa = 100$ kcal/mol in both collective variables and 500-ps-long trajectories at each center. We performed two-dimensional free energy reconstructions from this data (and from subsets thereof) using GPR(d) and LSRBF. In the GPR(d) reconstructions we used a length-scale hyperparameter of $l = \pi/3$ and prior function variance of $\sigma_f^2 = 20$ kcal$^2$/mol$^2$. In the four-dimensional system we used two interlocking grids of $6^4$ evenly spaced umbrella centres each (i.e. the second grid is obtained by translating the first by half a unit cell in all four directions) as well as a denser grid of $9^4$ evenly spaced centres, all with an umbrella strength of $\kappa = 400$ kcal/mol and running trajectories of 500 ps at each center.

### 3.2 Noise parameters

The GPR(d) requires an estimate of the noise variances for the measured mean forces, $\Sigma_{y'}$ in Eq. (7), which we calculate from the sample variance and effective number of independent samples, as discussed in Part I Sec. 3.2. The sample noise increases with increasing umbrella strength (due to equipartition), but a stiffer umbrella also reduces the non-uniformity of the grid of mean sample positions, which are displaced from the umbrella centres by amounts proportional to the local gradients and inversely proportional to the umbrella strength. We find that in the four-dimensional case, when data is intrinsically scarce, the stiffer umbrella we use ($\kappa = 400$ kcal/mol) gives better results than the softer one used in two dimensions.

## 4 Results

### 4.1 Two dimensions

Figure 1 shows the RMS gradient error in the reconstruction of the two dimensional free energy surface using the GPR(d) and the LSRBF methods. The error is given as the mean squared deviation of the analytical gradients of each reconstruction from the measurements

made on the densest $(48 \times 48)$ grid. We do find, as expected, that the condition numbers of the matrices in the LSRBF reconstructions are often very large indeed, at times exceeding values of $10^{18}$. This leads to an instability of the linear solver due to finite precision floating point arithmetic, which is easily controlled by employing a singular value decomposition (SVD). The bottom two panels of Fig. 1 show the variation of the RMS gradient error with the choice of length scale parameter for both the GPR(d) and LSRBF methods, as well as the variation of the square root of the quantity $E(\mathbf{a})$, defined in Eq. (3), for the LSRBF case. The latter is used in Ref. 5 to find an 'optimal' value for $l$.

Concerning the LSRBF reconstructions only, it seems clear that optimising the length-scale hyperparameter $l$ with respect to the data does not offer any advantage over a judicious choice of it. Indeed it can (particularly in the limit of scarce data) lead to very unphysical results, because it exacerbates the problem of overfitting. In fact, for chemistry and material systems it is usually not very difficult to choose an appropriate value of $l$ before the reconstruction is undertaken, taking note of the physical meaning of this hyperparameter: it is the correlation length of the free energy surface. For smooth functions in dihedral angles, setting the *a priori* correlation length to any value in $[\pi/3, \pi]$ is reasonable, as demonstrated by the relatively flat curves of the RMS gradient error for $l$ values in this range. We expect this to hold true for all free energy surfaces in dihedral angles of atomistic systems. As anticipated in Sec. 2, the discrepancy in performance between the two methods grows as the grid density decreases, i.e. as the data becomes more scarce. While the differences between the respective RMS gradient errors might not seem dramatic, the visualisations of the free energy surface reconstructions, shown in Fig. 2, underscore the advantages of GPR(d).

We further explored the relative performance of the two methods in the regime of high statistical noise. To this end, we reconstructed the free energy surface from successively shorter trajectories sampled on a grid of $144 = 12 \times 12$ umbrella centres. As the trajectory length decreases, the results obtained will show an increasing variance between runs. Fig. 3 shows the medians of the RMS reconstruction gradient errors obtained from 50 different

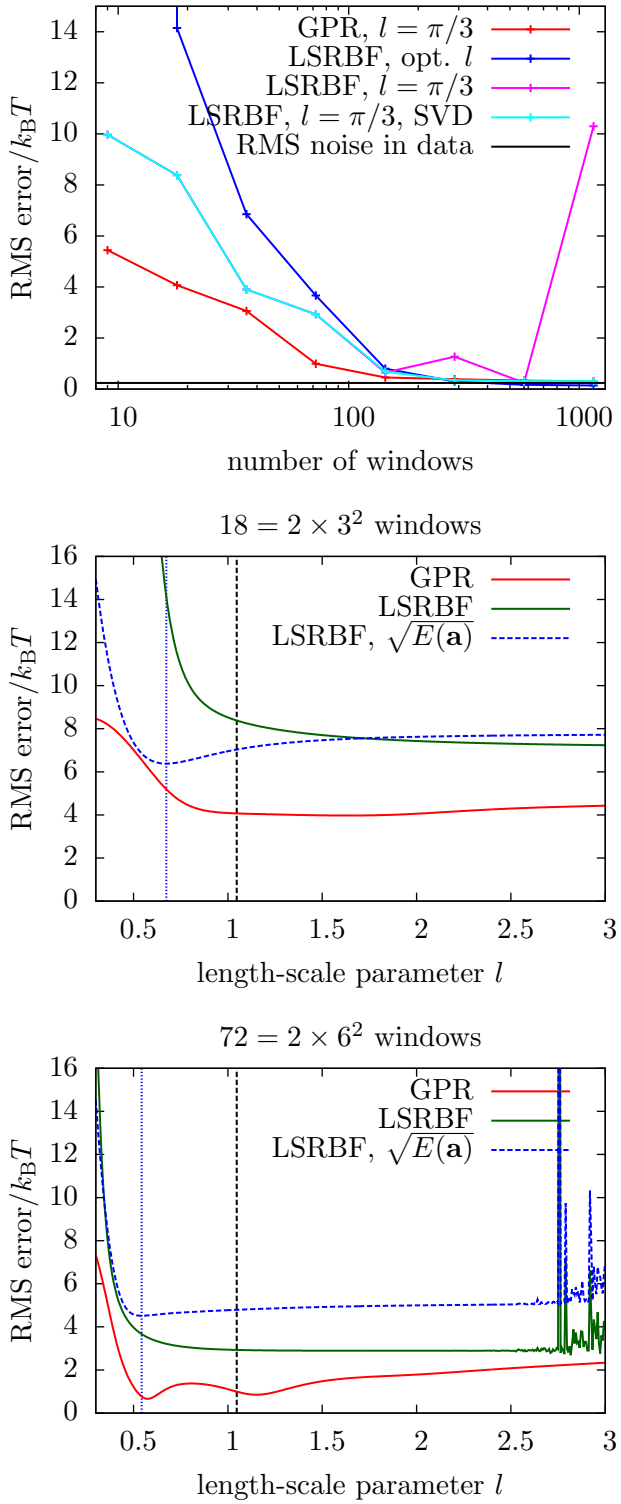


Figure 1: **Top panel**: RMS deviations of free energy gradients of alanine dipeptide reconstructed using LSRBF (with and without singular value decomposition to control the condition number) and GPR(d) in two dimensions. **Bottom two panels**: Variation of the RMS gradient error with the choice of length scale hyperparameter, $l$, for the GPR(d) and LSRBF in the case of 18 and 72 centres. Also shown is the quantity $\sqrt{E(\mathbf{a})}$ for the LSRBF reconstruction, used in Ref. 5 to optimise $l$; its 'optimal' value is marked by the dotted blue vertical line. The dashed black vertical line marks the value $l = \pi/3$ chosen *a priori* and used throughout the rest of this work.

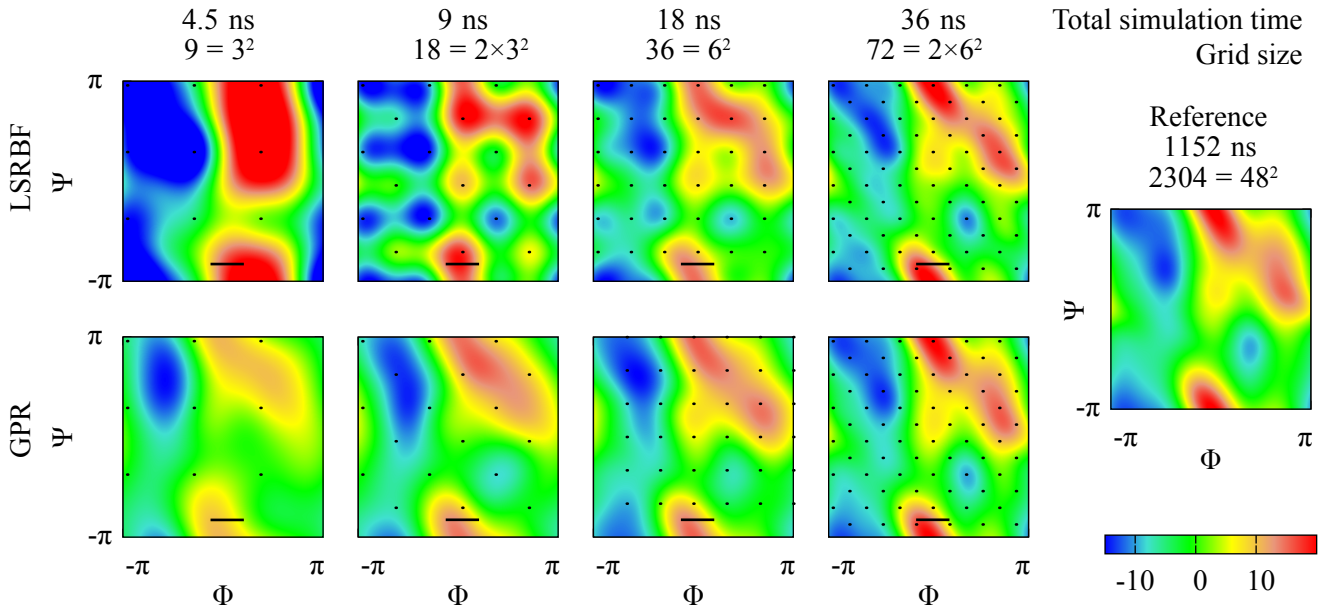


Figure 2: GPR(d) and LSRBF reconstructions of the free energy surface of alanine dipeptide in two dimensions using different numbers of umbrella centres, with a sampling trajectory of 500 ps/center. The reconstructions are visually indistinguishable when more than 72 centres are used. The free energy is given in units of $k_{\mathrm{B}}T$. The black dots mark the location of the umbrella centres used in the reconstructions. The black line segments indicate our choice of length-scale parameter $l = \pi/3$.

reconstructions with the same trajectory length. Also shown is an estimate of the breath of the distribution, the range between the 4th and the 96th percentile of the sample of reconstructions. To give a feel for the kind of reconstructions obtained from a trajectory of given length, Fig. 4 shows the reconstructions corresponding to the 96th percentile of the sample (the third-worst out of 50) for each trajectory length. We choose to show reconstructions from the worse end of the spectrum as they better highlight the resilience of the GPR(d) method to noisy input data. While the LSRBF reconstructions attempt to fit the data (including the noise) as closely as possible in a least squares sense, the GPR(d) reconstructions take the statistical noise into account, resulting in a greater resilience to it.

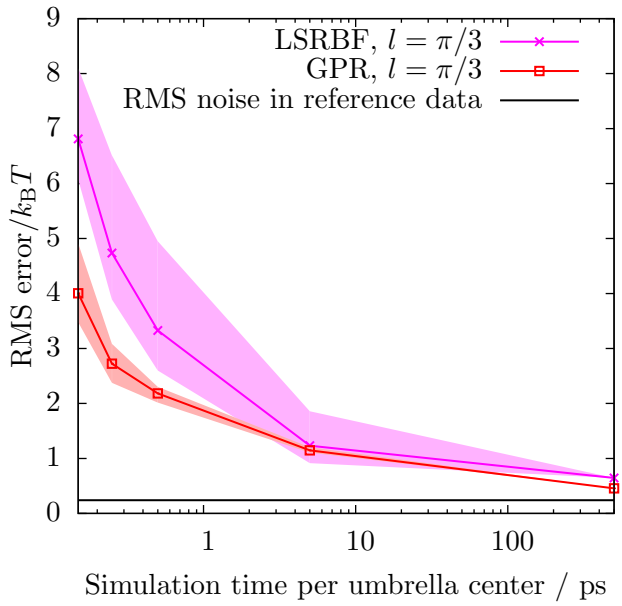


Figure 3: The median and the typical range of the RMS deviations in the reconstructed free energy gradients of alanine dipeptide. Samples of 50 reconstructions at each sampling time and method (LSRBF and GPR(d)) were used to calculate the median; the shaded area represents the range between the 4th and the 96th percentile of these samples (i.e. between the third best and third worst sample out of 50). All reconstructions use a grid of $12 \times 12$ umbrella centres, while the sampling time in each center is varied as shown.

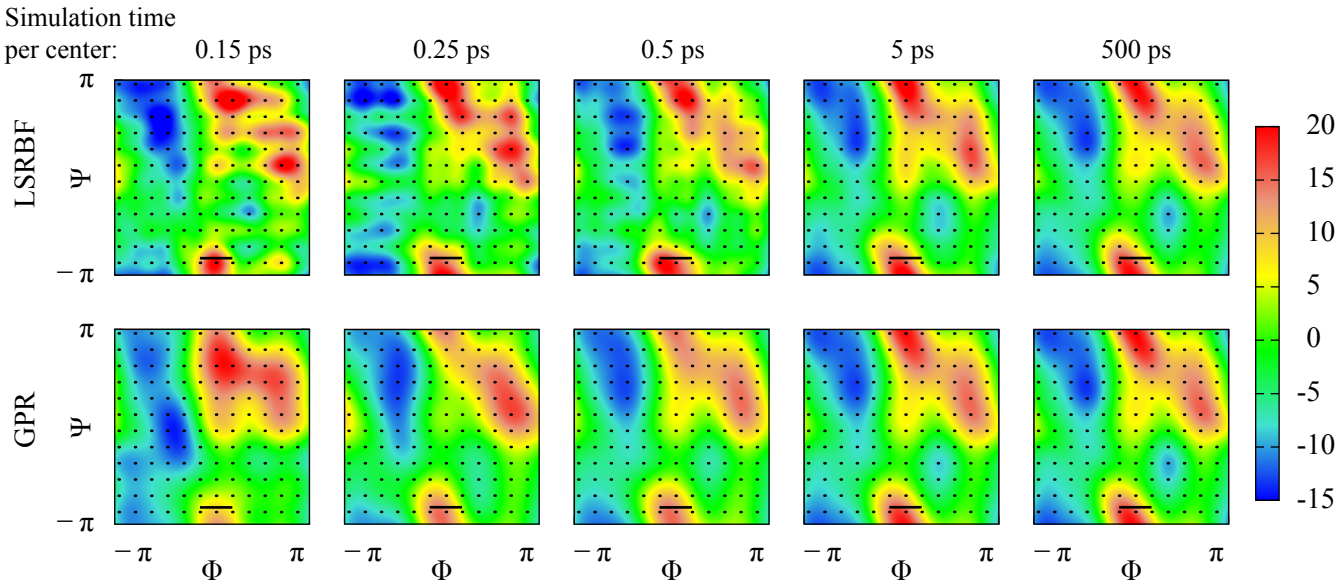


Figure 4: GPR(d) and LSRBF reconstructions of the free energy surface (in units of $k_{\mathrm{B}}T$) of alanine dipeptide in two dimensions from data gathered in $12 \times 12$ umbrella centres (the centres are marked by black dots) over a varying sampling time. Shown are the reconstructions with the third-largest RMS gradient errors from a sample of 50 (representing the 96th percentile) for each sampling time. The black line segments indicate the magnitude of the length-scale parameter $l$.

## 4.2 Four dimensions

Finally, we compared the performance of the two methods in four dimensions, where data is necessarily much scarcer. Fig. 5 shows the RMS deviations of free energy gradients obtained from reconstructions using various subsets of these data sets with respect to reference data obtained on a denser grid of $9^4$ evenly spaced umbrella centres. GPR(d) outperforms the LSRBF fit, but even using more than 2000 umbrella centres GPR(d) has a remaining gradient error of about $k_{\mathrm{B}}T$. The LSRBF, on the other hand, fails to provide a reconstruction better than 10 $k_{\mathrm{b}}T$ even when using the densest grid.

Fig. 6 shows 2D slices of these reconstructions at values of -2.0 and 2.0 for the third and fourth backbone dihedral angles (counted from the N-terminal end), respectively. These slices are compared to a reference 2D reconstruction based on data sampled on a 2D grid of $48 \times 48$ centres in the plane concerned. For large numbers of centres both methods result in acceptable looking reconstructions, with GPR(d) converging to the reference. However, only

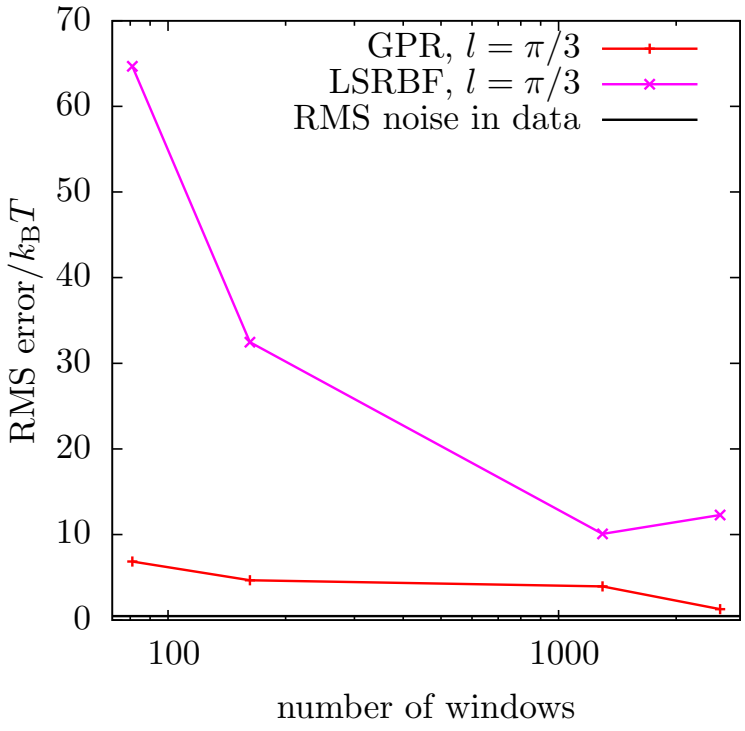


Figure 5: RMS deviations of free energy gradients reconstructed using LSRBF and GPR(d) in four dimensions from subsets of $2 \times 6^4$ free energy gradient observations, with respect to a reference set of $9^4$ free energy gradients.

the GPR(d) fit remains qualitatively reasonable for small numbers of centres. The larger gradient error of the LSRBF reconstruction, especially for small numbers of centres, seen in Fig. 5 is accompanied by prominent artefacts centered on the sampling points visible in Fig. 6.

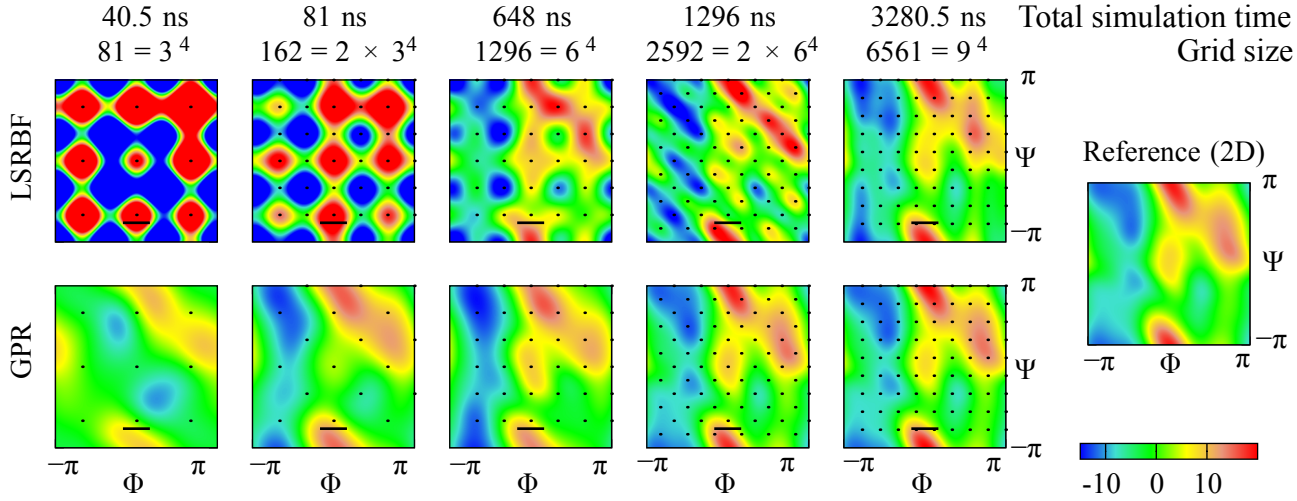


Figure 6: 2D slices of GPR(d) and LSRBF reconstructions of the free energy surface (in units of $k_{\mathrm{B}}T$) of alanine tripeptide using different numbers of umbrella centres, at third and fourth backbone dihedrals (from the N-terminus) of -2.0 and 2.0, respectively. $\Phi$ and $\Psi$ refer to the first two backbone dihedrals from the N-terminus, respectively. The black dots mark the centres of the umbrella centres, projected onto the 2D slice of the reconstruction. The black line segments indicate the magnitude of length-scale parameter $l = \pi/3$.

# 5 Conclusions

In this paper we investigated the use of Gaussian process regression using gradient data in the reconstruction of free energy surfaces in two and four collective variables. We highlighted both the similarities and essential differences between the GPR(d) and the popular reconstruction method of least squares fitting with radial basis functions. Both methods can be understood to take an ansatz that is a linear combination of basis functions. However, while the latter approach places a radial basis function with its maximum on each data point, GPR(d) uses the gradients of these functions in its expansion of the free energy. Not only

are the gradient functions better suited to represent the gradient data, there is also a greater number of them (one gradient function for every collective variable), giving GPR(d) greater flexibility.

The second key difference between GPR(d) and the LSRBF approach is the way in which the expansion coefficients are calculated. GPR(d) is a Bayesian method and takes account of both our prior assumption of smoothness and the noise associated with the data in a consistent way. The LSRBF method, on the other hand, is prone to overfit the data. These differences become particularly apparent in the limits of spatially scare data and also of short sampling trajectories (i.e. high statistical noise) but reasonably dense umbrella centres, where GPR(d) is shown to outperform the LSRBF approach both visually and numerically. Finally, in a regime of spatially dense data, GPR(d) avoids the very large condition numbers often associated with LSRBF methods by adding the noise matrix to the linear system.

## Acknowledgement

We thank Eric Vanden-Eijnden for comments on the manuscript. N.B. acknowledges funding for this project by the Office of Naval Research (ONR) through the Naval Research Laboratory's basic research program. G. C. Office of Naval Research under Grant No. N000141010826 and from the European Union FP7-NMP programme under Grant No. 229205 "ADGLASS".

## References

(1) Rasmussen, C. E.; Williams, C. K. I. *Gaussian Processes for Machine Learning (Adaptive Computation and Machine Learning series)*; MIT Press, 2005.

(2) Laio, A.; Parrinello, M. *Proc. Natl. Acad. Sci. U.S.A.* **2002**, *99*, 12562–12566.

(3) Darve, E.; Pohorille, A. *J. Chem. Phys.* **2001**, *115*, 9169–9183.

(4) Darve, E.; Rodriguez-Gomez, D.; Pohorille, A. *J. Chem. Phys.* **2008**, *128*, 144120.

(5) Maragliano, L.; Vanden-Eijnden, E. *J. Chem. Phys.* **2008**, *128*, 184110.

(6) Maragliano, L.; Vanden-Eijnden, E. *Chem. Phys. Lett.* **2006**, *426*, 168–175.

(7) Rosso, L.; Minary, P.; Zhu, Z.; Tuckerman, M. E. *J. Chem. Phys.* **2002**, *116*, 4389–4402.

(8) Abrams, J. B.; Tuckerman, M. E. *J Phys Chem B* **2008**, *112*, 15742–15757.

(9) Chen, M.; Cuendet, M. A.; Tuckerman, M. E. *J. Chem. Phys.* **2012**, *137*, 024102.

(10) Buhmann, M. D. *Acta Numerica* **2000**, *9*, 1–38.

(11) Mackay, D. J. C. *NATO ASI Series F Computer and Systems Sciences* **1998**, *168*, 133–166.

(12) MacKerell, A.; Bashford, D.; Bellott, M.; Dunbrack, R.; Evanseck, J.; Field, M.; Fischer, S.; Gao, J.; Guo, H.; Ha, S.; Joseph-McCarthy, D.; Kuchnir, L.; Kuczera, K.; Lau, F.; Mattos, C.; Michnick, S.; Ngo, T.; Nguyen, D.; Prodhom, B.; Reiher, W.; Roux, B.; Schlenkrich, M.; Smith, J.; Stote, R.; Straub, J.; Watanabe, M.; Wiorkiewicz-Kuczera, J.; Yin, D.; Karplus, M. *J Phys Chem B* **1998**, *102*, 3586–3616.

(13) Schneider, T.; Stoll, E. *Phys. Rev. B* **1978**, *17*, 1302–1322.

(14) Plimpton, S. *Journal of Computational Physics* **1995**, *117*, 1–19.

(15) Bonomi, M.; Branduardi, D.; Bussi, G.; Camilloni, C.; Provasi, D.; Raiteri, P.; Donadio, D.; Marinelli, F.; Pietrucci, F.; Broglia, R. A.; Parrinello, M. *Comput. Phys. Commun.* **2009**, *180*, 1961–1972.